Soft Matter

PAPER

View Article Online
View Journal | View Issue

Cite this: *Soft Matter*, 2024, **20**, 4583

Poroviscoelastic relaxations and rate-dependent adhesion in gelatin†

Wonhyeok Lee and Melih Eriten*

Received 16th March 2024,
Accepted 2nd May 2024

DOI: 10.1039/d4sm00318g

rsc.li/soft-matter-journal

Hydrogels, polymeric networks swollen with water, exhibit time/rate-dependent adhesion due to their poroviscoleastic constitution. In this study, we conducted probe-tack experiments on gelatin and investigated the influence of dwelling times and unloading rates on pull-off forces and work of adhesion. We utilized *in situ* contact imaging to monitor separation kinematics and interfacial crack velocities. We found that the crack velocities scaled nonlinearly with the unloading rate, in a power law with an exponent of 0.8 and were independent of dwelling time. At maximum unloading rates corresponding to subsonic interfacial crack speeds, we observed an order of magnitude enhancement in the apparent work of adhesion. The enhancement of adhesion and the crack velocities were related by a power law with an exponent of 0.39. The maximum vertical extension during unloading, a measure of crack opening, exhibited linear correlation with the enhancement of adhesion. Both correlations were in line with the rate-dependent work of fracture modeled for viscoelastic solids (*e.g.*, Persson and Brener model). We explored the links between dwelling times corresponding to varying degrees of poroelastic diffusion and the adhesion. We found 40% additional enhancement in adhesion at the highest unloading rate. This enhancement is due to the unbalanced osmotic pressure, also known as the suction effect. The influence of dwelling times on adhesion was negligible for the interfacial cracks propagating slower than the diffusive time scales. These results identify viscoelastic relaxations as the dominant mechanism governing the rate-dependent enhancement of adhesion, and hence pave the way for tuning rate-dependent adhesion in soft multiphasic materials.

1 Introduction

Hydrogels are poroviscoelastic (PVE) materials that consist of polymer networks swollen with water.[1] These polymer networks can be formed by physical or chemical crosslinks.[2] When deformed, these polymer networks exhibit a time-dependent stress–strain response and PVE relaxations;[3,4] the polymer chains reconfigure and reach a new equilibrium: viscoelastic relaxation, and the solvent diffuses through the polymer networks due to the pressure gradient: poroelastic relaxation.[5,6] In a PVE material, these relaxations can occur concurrently[7] and influence adhesion and fracture. For instance, several studies have explored the influence of contact time on adhesion in hydrogels,[8–11] cartilage,[12] mucin gels[13] and adhesives on hydrated biological tissues.[14] These studies have reported that adhesion increases with contact (holding/dwelling) time thanks to the suction effect caused by an unbalanced osmotic pressure over the contact.[9,13,15] Moreover, Michel *et al.*[10] demonstrated that with contact time, freely available water over the contact between a dry hydrogel film and liver tissue transports into the hydrogel. This leads to enhanced solid–solid contact and adhesion. A similar adhesion mechanism was proposed by Lai *et al.*[16] where the amount of polymer chains adhering to the counter surface and thus pull-off forces increase with contact time. Moreover, adhesion measured on PVE materials depends on unloading rates as observed in cartilage,[15] insect feet,[17] oil-swollen foams,[18] and epithelial cells.[19] For explaining the rate-dependence, fracture and adhesion mechanics of viscoelastic solids has been promising. However, due to deformation kinematics local to contact edges[20–23] or viscoleastic dissipation[24–26] during peeling, higher unloading rates are shown by these models to increase the apparent work of adhesion in viscoelastic materials. The mechanisms governing the contact time and rate-dependent adhesion in PVE materials are more complicated as diffusion and relaxation mechanisms can be coupled. In this work, we will examine the adhesion of gelatin on a glass probe at broad time scales relevant to PVE relaxations. This way, we hope to decouple the influences of poroelastic diffusion and viscoelastic relaxations, and obtain dominant mechanisms leading to rate-dependent adhesion in multiphasic materials.

In particular, we conduct adhesion tests on gelatin at various unloading rates and hold times that trigger only

Department of Mechanical Engineering, University of Wisconsin-Madison, Madison, WI, USA. E-mail: eriten@wisc.edu

† Electronic supplementary information (ESI) available. See DOI: https://doi.org/10.1039/d4sm00318g

non-inertial response of the gels; *i.e.*, crack (contact edge) velocities remain much lower than shear wave velocity. We also characterize PVE time constants, and correlate the enhancement of gel adhesion to the degree of relaxation. Besides, we capture contact images to analyze contact kinematics, and its link to local viscoelastic response and thus enhancement of adhesion. Our results indicate that the PVE response localized under the rigid probe leads to an order of magnitude increase in the apparent work of adhesion. Furthermore, this enhancement correlates well with contact kinematics such as crack velocities and tip (contact edge) opening during separation. These observations corroborate well with the scaling laws predicted by existing crack propagation theories in viscoelastic materials. The so-called suction effect due to increasing dwelling times has a second order effect on adhesion compared to the viscoelastic enhancement. These results are essential for better understanding and control of adhesion in soft multiphasic materials.

2 Methods and analyses

2.1 Sample preparation

Gelatin samples are prepared by blending 5 w/v% of gelatin powder from porcine skin (G2500 Type A, Sigma Aldrich, Inc.) with water. This concentration is chosen considering the transparency and stiffness required for the imaging module, contact size, and load cell specifications. The blend is heated to 60 °C and mixed at 150 rpm for 30 minutes to achieve a homogeneous solution. The solution is then cooled to 45 °C while being stirred under ambient conditions. To remove bubbles from the solution, it is placed in a vacuum chamber (1.5 gal, Vevor) connected to a vacuum pump (3.6 CFM, 1/4 HP, Vevor). The pressure is kept at 20 kPa until all visible bubbles in the solution have been removed. Then, the solution is poured into a Petri dish (50 mm radius and 15 mm thickness) and cured in a refrigerator for 2 hours at 5 °C. Before mechanical testing, the sample is allowed to equilibrate at room temperature (T = 23 °C) for 10 minutes.

2.2 Adhesion tests

Adhesion tests are conducted in a custom-built probe tack tester, sketched in Fig. 1(a). A motorized linear actuator (VT-75, Physik Instrumente, 2 μm resolution) is used to apply the normal displacement δ in y direction. A stiff bar extending from the actuator carries a low-capacity miniature S-beam load cell (LSB200, 10 g capacity, FUTEK, Inc, 50 μN resolution) to measure the normal force F and a plano-convex glass lens (Edmund Optics, Inc.) with a tip radius of R = 10.54 mm to be used as the probe. The

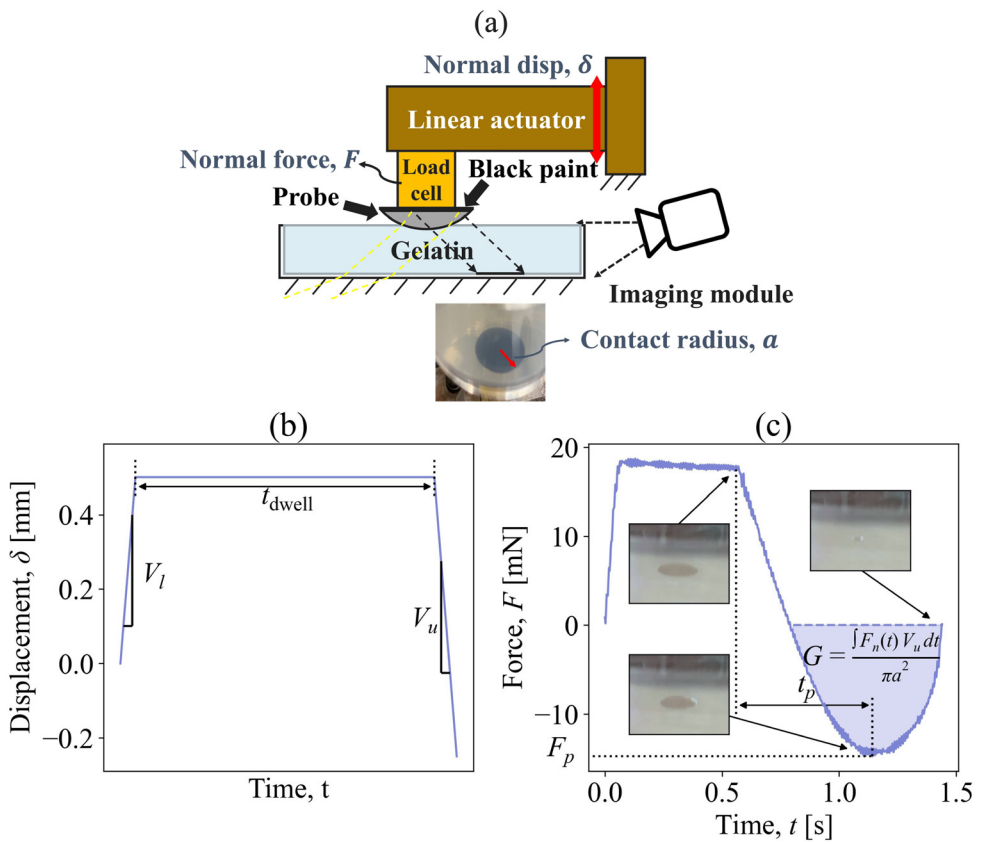

Fig. 1 (a) The sketch of the experimental setup and a contact image captured with the imaging module, and (b) a representative normal displacement δ profile used in the adhesion experiments. The loading rate of V_l = 10 mm s^{-1}, the unloading rates of V_u = {0.01, 0.1, 1, and 10} mm s^{-1}, and the dwell times of t_{dwell} = {0.5, 100, and 200} s are used in the experiments. (c) A representative force measurement obtained from the adhesion experiment at a dwelling time of t_{dwell} = 0.5 s and unloading rates of 1 mm s^{-1}. Inset figures in (c) show the evolution of the contact area during unloading corresponding to the beginning of unloading, pull-off, and right before full-separation. The contact radius at the beginning of unloading is 2.9 mm.

probe is impermeable and can be assumed rigid thanks to the six order of magnitude contrast in glass and gel moduli. The plane-side of the probe that is attached to the load cell has a radius of 6.35 mm.

Before each test, we center and fix the sample below the probe. Then, we lower the probe until the first moment of contact as detected by the contact imaging (see Section 2.3 for details). Once the surface is identified, the probe is retracted to a close but noncontact position relative to the sample surface. The surface detection step enables faster loading and consistent contact areas during dwelling portion of the actual adhesion tests. The actual adhesion tests consist of three steps: loading, dwelling and unloading, as depicted in Fig. 1(b). Initially, the probe is indented into the surface by 0.5 mm at 10 mm s^{-1}. The loading duration $\sim$0.05 s is much smaller than the viscoelastic relaxation time constant τ_{VE} = 0.222 s, as estimated from the relaxation response (see Section S1 of the ESI†). An indentation of 0.5 mm results in a contact radius $a \approx$ 2.9 mm, as measured with the contact imaging module. Given that the contact radius is significantly smaller than the dimensions of the gelatin sample (50 mm radius and 15 mm thickness), the boundary effects are negligible. After loading, the probe is held stationary at 0.5 mm displacement for dwelling times t_{dwell} = 0.5, 100 and 200 s. During this time, the hydrogels' solid networks reconfigure quickly (viscoelastic relaxation) under deformation, while the water diffuses slowly away from the highly stressed contact zone (poroelastic relaxation). Since we conduct all testing under ambient conditions, dehydration of the gelatin samples is inevitable. To limit water losses to within 5 wt%, we finish all testing within a few hours. That is why we set the longest dwelling time to 200 s. Note that we measure the poroelastic time constant as 87.3 s (see Section S1 of the ESI†) and so 90% of the poroelastic relaxation occur within 200 s, and this enables us to study the influence of broad degree of poroelastic relaxations on adhesion. At the end of the dwelling period, the probe is retracted until complete separation, at different unloading rates V_u = 0.01, 0.1, 1, and 10 mm s^{-1}. The lower bound of unloading rate V_u = 0.01 mm s^{-1} is determined considering the enhancement of work of adhesion. In preliminary experiments, the apparent work of adhesion at $V_u < 0.01$ mm s^{-1} shows a similar value to the one at V_u = 0.01 mm s^{-1}. The upper bound V_u = 10 mm s^{-1} is chosen to ensure that the crack velocity is sufficiently below the shear wave speed of gelatin $V_s \sim 2$ m s^{-1}, thereby restricting our experiments to the range of subsonic cracks and non-inertial material response. Between each test, we allow the sample to equilibrate for $t_{break} > t_{dwell}$ and monitor its weight to ensure that the sample does not undergo more than 5 wt% dehydration.

We repeat adhesion tests four times for each dwelling time and unloading rate (totally 48 tests), while monitoring the normal force F at a sampling frequency of 400 Hz. Fig. 1(c) presents an example of force measurements from the adhesion tests at 0.5 s dwelling time and 1 mm s unloading rates. From these measurements, we extract the pull-off force F_p and the apparent work of adhesion G as a measure of adhesive strength. As shown in Fig. 1, we estimate the latter by equating the apparent work needed for full separation to the tensile work done on the probe; *i.e.*, $\pi a^2 G = V_u \int F_n dt$.

2.3 Contact imaging and kinematics

During the adhesion tests, we capture videos of the contact from a tilted position above the sample at 30 fps for 0.01 mm s^{-1} and 0.1 mm s^{-1} unloading cases, and at 240 fps for 1 mm s^{-1} and 10 mm s^{-1} with 20 μm per pixel resolution, using a smartphone camera (Fig. 1(a)). Black paint applied to the plane-side of the probe absorbs light and thus provide a dark/bright contrast between contacting and non-contacting parts of the gel surface. For instance, the inset figures in Fig. 1(c) show images of the contact region at an unloading rate of V_u = 1 mm s^{-1} and a dwelling time of t_{dwell} = 0.5 s. In Fig. 1(c), the inset figures correspond to the start of unloading, the maximum pull-off force F_p, and right before complete separation, respectively. Because of the tilted camera view, the contact areas appear elliptical instead of circular. Nevertheless, we calibrated the camera images against known physical lengths along the center of the sample so that we could record contact diameter, $2a$, as the length of the major axis of the ellipse. Note that in addition to the poroviscoelastic relaxation time scales, there is another time scale at which delayed contact peeling (crack opening) or formation (crack closure) can occur in rate-dependent materials.[27] For soft materials at the mm contact sizes, the time scale is orders of magnitude larger than the poroviscoelastic time constants that we observed in gelatin. Hence, we have not observed any significant change in contact area during the dwelling portion of our tests. We track the evolution of contact radii over the duration of unloading and then define the crack velocity $V_c = |da/dt|$ at the instance of pull-off. To lessen the influence of noise, a spline derivative with a smoothing parameter s = 5 is used to compute the crack velocities.

3 Results and discussion

3.1 Enhancement of gel adhesion

Fig. 2(a) and (b) illustrate the variation in pull-off force F_p and apparent work of adhesion G as a function of unloading rate V_u at different dwelling times. As a measure of repeatability, four repetitions of each case are encapsulated in the shaded strips. The apparent work of adhesion G = 74.8 mJ m^{-2} that we measured at t_{dwell} = 0.5 s and V_u = 0.01 mm s^{-1} is comparable to the thermodynamic work of adhesion $\Delta\gamma \sim 85$ mJ m^{-2} found by Khakalo *et al.*[28] for a type A porcine skin gelatin ($\sim$10 to 20 w/v%). Therefore, we will take G = 74.8 mJ m^{-2} as a reasonable estimate of thermodynamic work of adhesion $\Delta\gamma$ in the upcoming analysis. The largest apparent work of adhesion that we recorded is G = 886 mJ m^{-2}, which is about one-third the cohesive strength reported as the fracture energy ($\sim$2500 mJ m^{-2}) by Baumberger *et al.*[29] for a type A porcine skin gelatin (5 w/v%) at quasistatic crack velocities.

Both adhesion measures reveal strong enhancement with unloading rates V_u; *e.g.*, $\sim$5-fold and 10-fold increase in pull off force and apparent work of adhesion, respectively. Increasing

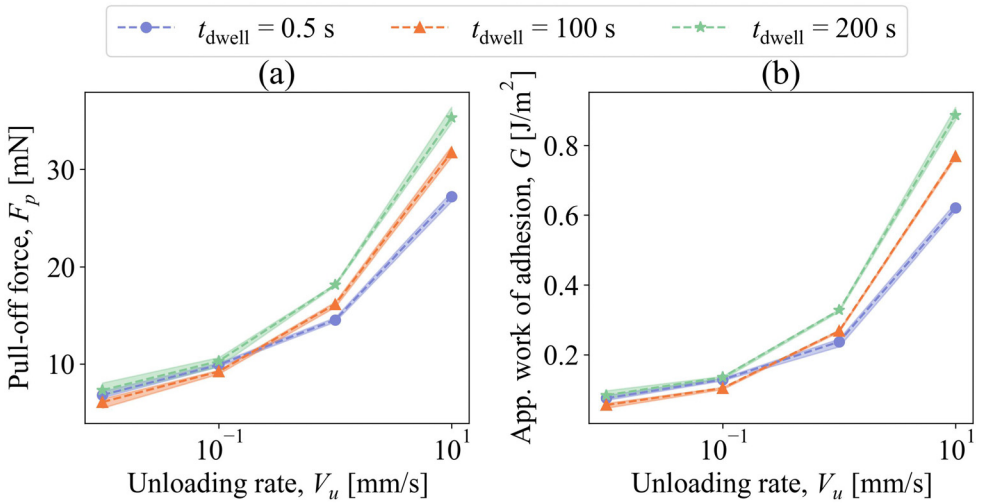

Fig. 2 Results of the adhesion experiments: (a) the pull-off force F_p plotted against the unloading rate V_u. (b) The apparent work of adhesion G plotted against the unloading rates. The shaded area in the plots represents the range between the maximum and minimum values.

dwelling times t_{dwell} contributes to this enhancement but rather weakly compared to the unloading rates. This dependence on the unloading rate and dwelling time is in line with previous observations in ref. 11 and 30 where more than an order of magnitude increase in work of adhesion (from 60 to 1000 mJ m^{-2}) was obtained in Milli-Q water between the poly(MAETAC-*co*-AAm) hydrogel and a PAA hydrogel thin film when the unloading rate was increased from 1 to 1000 μm s^{-1}. The same authors also found that increasing the contact time from 1 to 1200 s leads to a 2-fold increase in work of adhesion of the same materials. The maximum enhancement that we observed due to increasing dwelling time is 40%; *e.g.*, the apparent work of adhesion G increases from 621 to 886 mJ m^{-2} at V_u = 10 mm s^{-1}, as t_{dwell} increases from 0.5 to 200 s. The glass-probe on gel configuration that we tested can lead to different contact physics, especially poroelastic effects when compared to the gemini configuration studied in ref. 11. Similar configuration-dependent differences were observed in friction and lubrication properties of polyacrylamide gels.[31]

3.2 Viscoelastic enhancement

Contact kinematics and its dependence on unloading rates and dwelling times could potentially explain the enhancement observed in adhesion. We plot the evolution of contact radius during the unloading stage of the tests at t_{dwell} = 0.5 s for different unloading rates in Fig. 3(a). For illustration purposes, time is normalized by t_p, where t_p = {57.2, 6.20, 0.588, and 0.143} represent the duration from the start of unloading to the

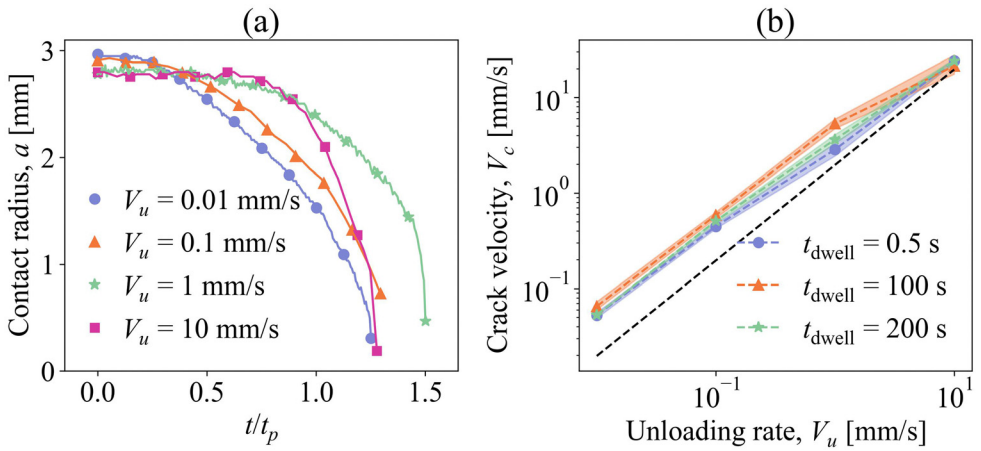

Fig. 3 Representative (a) evolution of the contact area a as a function of time t during unloading at a dwelling time of t_{dwell} = 0.5 s. The values of t_p = {57.2, 6.20, 0.588, and 0.143} correspond to unloading rates of V_u = {0.01, 0.1, 1, and 10} mm s^{-1}, respectively, where t_p is the time when $F = F_p$. (b) The theoretical (represented by the dashed line) crack velocity obtained from the viscoelastic JKR model and experimentally estimated (represented by the scatter plot) crack velocity V_c as a function of the unloading rate V_u. The shaded area in the plots represents the range between the maximum and minimum values.

instant when pull-off force F_p is reached. Since time is normalized, the slope of Fig. 3(a) is scaled with t_p. Notably, contact radii at pull-off $a_{t=t_p}$ are larger for larger unloading rates. This observation corroborates the numerical work by Afferrante *et al.*[32] Fig. 3(b) shows the crack velocities $|da/dt|_{t=t_p}$ measured at different V_u and t_{dwell} values of 0.5, 100, and 200 s. The crack velocities range from 0.05 to 30 mm s^{-1} residing well below the sonic regime. Besides, the crack velocities exhibit approximately power law scaling with the unloading rates; *i.e.*, $V_c \propto V_u^{0.8}$. To inspect it quantitatively, we project on Fig. 3(b) the theoretical crack velocities estimated *via* the viscoelastic JKR model after Greenwood and Johnson:[23,33,34]

$$V_c = \left|\frac{da}{dt}\right| = \left|\frac{da}{d\delta}\frac{d\delta}{dt}\right| = \left|\frac{da}{d\delta}V_u\right| = V_u \Big/ \left(\frac{2a}{R} - \sqrt{\frac{\pi\Delta\gamma}{2aE^*}}\right) \quad (1)$$

Here, the apparent work of adhesion $G = 74.8$ mJ m^{-2} estimated at $t_{dwell} = 0.5$ s and $V_u = 0.01$ mm s^{-1} is used for $\Delta\gamma$, $E^* = E/(1-\nu^2) = 12.5$ kPa is the reduced modulus estimated from the gel's response to initial loading, and $a = 2.9$ mm is imaged at the start of unloading. Since the denominator of the last expression of eqn (1) is independent of V_u, the theory predicts $V_c \propto V_u$, which is very close to the power law that we obtained experimentally. Besides, quantitative match between the theoretical and experimental contact kinematics suggests the dominance of viscoelastic crack propagation in the unloading phase of the adhesion tests. This is also reflected in the weak dependence of crack velocities to t_{dwell} and thus poroelasticity. We then compute Deborah number De = {0.004, 0.034, 0.216, and 1.842} as $\tau_{VE}/(a/V_c)$, which is a measure of the fluidity of materials at different unloading rates V_u = {0.01, 0.1, 1, and 10} mm s^{-1}. We assume that $a = 2.9$ mm is constant for all cases, and V_c is independent of t_{dwell} for the calculation of De. a/V_c is the average time it takes for the crack to propagate over the whole contact. For the slowest unloading $V_u = 0.01$ mm s^{-1}, the crack propagates very slowly compared to the viscoelastic relaxation, resulting in De $\ll 1$ and expectedly a fully-relaxed material behavior. In contrast, at the fastest unloading rate $V_u = 10$ mm s^{-1} case, the crack opening is faster than viscoelastic relaxation, and the material in the vicinity of contact acts like an unrelaxed elastic solid during unloading. This wide range of expected viscoelastic response prompted us to further inspect crack propagation in viscoelastic media.

For instance, Persson and Brener[25] assume that the energy flow to the crack tip can be considered as the apparent work of fracture and can be expressed as the sum of work of fracture and viscoelastic dissipation. Since the latter stems from dissipation capacity of the viscoelastic material (say loss modulus), which itself depends on strain rates, apparent work of fracture is found to change with crack velocity. Applying this idea to the power-law relaxation response commonly-observed for rubber compounds between rubbery and glassy time scales, Persson and Brener listed the following relationship for the enhancement of work of fracture and crack velocities for various viscoelastic models:

$$\beta_W = \frac{G}{\Delta\gamma} \sim \left(\frac{V_c}{V_{c,0}}\right)^{\alpha} \quad (2)$$

Here, $V_{c,0} \ll V_c$ is the characteristic velocity that determines the lower end of strain rates (frequencies) involved in crack propagation as $V_{c,0}/r_0$, and r_0 is the crack tip radius for quasistatic crack propagation. Note that a similar enhancement of work of fracture with crack velocities was shown experimentally on gelatin samples.[1,35] Taking multiple relaxations into account in dynamic modulus $E(\omega)$ of the viscoelastic material:

$$\frac{1}{E(\omega)} = \frac{1}{E_\infty} + \int_0^\infty \frac{H(\tau)}{1 - i\omega\tau} d\tau \quad (3)$$

Persson and Brener predicted the scaling power in eqn (2) $\alpha = (1-s)/(2-s)$ where $H(\tau)$ is the real and positive spectral density function of relaxation times τ; and the viscoelastic solid exhibits power-law relaxation with $H(\tau) \sim \tau^{-s}$, and $0 < s < 1$. The power-law relaxation response is known to hold for transition from

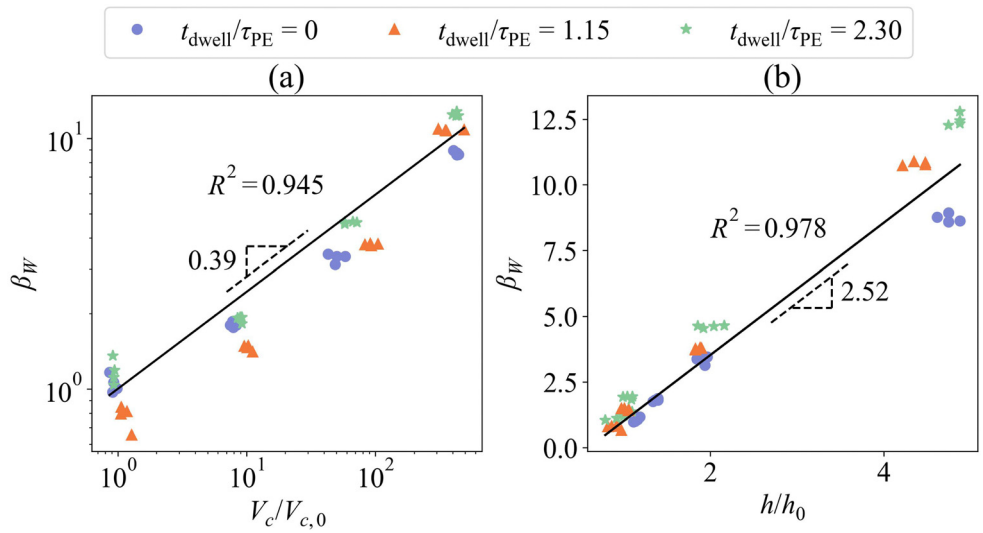

Fig. 4 Correlation of (a) the enhancement of work of adhesion with the crack velocity ($\beta_W \sim (V_c/V_{c,0})^{0.39}$ with $R^2 = 0.945$), and (b) the enhancement of work of adhesion with the vertical extension ($\beta_W \sim h/h_0$ with $R^2 = 0.978$).

glassy to rubbery response regimes, as well as for critical sol–gel transitions in gels.[36,37] Using eqn (3), one can show that $E(\omega) \sim \omega^n$ in those transition regimes with $n \sim 1 - s$. Typically, $n \approx 0.5$ for gelation with excessive crosslinks, and n = 0.6 to 0.7 for gelation without chemical crosslinks.[37] Experimentally, n is found to range from 0.5 to 0.7 for gelatin 5–10 w/v% at room temperature.[3,38–40] This range of n values corresponds to the scaling power α ranging from 0.33 to 0.41. In Fig. 4(a), we plot β_W as a function of $V_c/V_{c,0}$ for all 48 measurements, and obtain a scaling power of 0.39 ($V_{c,0}$ is the average of crack velocities obtained at the slowest unloading case). So, the rate-dependent enhancement that we measured in work of adhesion resides within Persson and Brener's power-law scaling of rate-dependent work of fracture. The scaling law given in eqn (2) applies also for narrower relaxation spectra. For instance, scaling power α = 0.5 for standard linear solids with a single time constant τ_0; *i.e.*, $H(\tau) \sim \delta(\tau - \tau_0)$.[25,41] With the current setup, we measured the relaxation response (see Section S1 of the ESI†) and identified a single relaxation time constant τ_{VE} to explain the evolution of force at time scales much shorter than poroelastic time constant τ_{PE}. However, an improved tester (rheometer) is needed to monitor relaxations at broader time scales, and obtain a possible power-law relaxation spectrum (see for instance[38,39]). To the best of our knowledge, a thorough study that investigates the links between the relaxation spectrum and rate-dependent adhesion is missing in the literature. Our findings in line with the Persson and Brener model propose a direct link.

The Persson and Brenner model also predicts that the increase in crack tip radius r is linearly proportional to the enhancement of work of fracture of viscoelastic materials; *i.e.*, $\beta_W \propto r/r_0$ regardless of the relaxation spectrum. In our experiments, we use the displacement history and tilted view of the imaging module to estimate the maximum vertical extension of gel h before full separation (see Section S2 of the ESI† for more details). We use the vertical extension as a measure of crack tip radius r due to the difficulties in measuring the crack tip radius with the current imaging module. In Fig. 4(b) we plot β_W as a function of h/h_0 for all 48 measurements (h_0 is the average of vertical extensions obtained at the slowest unloading case). Enhancement in work of adhesion correlates linearly with the vertical extensions, re-confirming that viscoelastic deformations, associated dissipation and crack tip kinematics can explain the observed rate-dependence of adhesion. Scaling of enhancement of adhesion with crack velocities and vertical extensions changes negligibly with t_{dwell} suggesting second order influence of poroelastic diffusion on rate-dependent adhesion. More discussion of that subtle influence will follow in Section 3.3.

3.3 Poroelastic enhancement

To better understand the influence of poroelastic diffusion, we plot in Fig. 5 β_F and β_W as a function of t_{dwell}/τ_{PE} for different De = $\tau_{VE}/(a/V_c)$. The term t_{dwell}/τ_{PE} can be thought of as the reciprocal of Péclet number (Pe), quantifying the extent of solvent migration away from the contact region during dwelling. We observe more enhancement of the work of adhesion as t_{dwell}/τ_{PE} increases at $\tau_{VE}/(a/V_c)$ = 1.842 and 0.216. On the other hand, at $\tau_{VE}/(a/V_c)$ = 0.004 and 0.034, the enhancement of work of adhesion is nearly independent of t_{dwell}/τ_{PE} and shows almost constant values. The effect of t_{dwell} on gel adhesion can be explained by the suction effect.[9] As the dwelling time increases, the solvent under the contact slowly diffuses away until a new equilibrium state is reached.[6] This diffusion creates a difference in concentration, leading to the buildup of a pressure gradient in longitudinal direction under the contact. Consequently, more force and energy are required to separate the surfaces. For slow unloading cases, the effect of dwelling time on adhesion is minimal. This is because the solvent that diffused away from the contact area has sufficient time to diffuse back and balance the pressure gradient caused by unloading; *i.e.*, negligible suction effect. On the other hand,

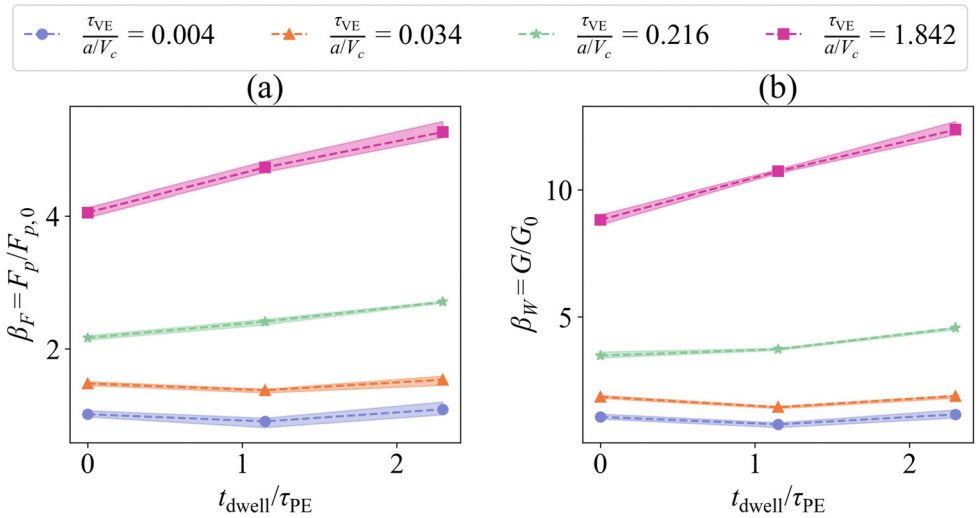

Fig. 5 The enhancement of adhesion as a function of the normalized holding time t_{dwell}/τ_{PE}, based on (a) pull-off force F_p and (b) apparent of work of adhesion G at different $\tau_{VE}/(a/V_c)$. The shaded area in the plots represents the range between the maximum and minimum values.

at higher unloading rates V_u = 1 and 10 mm s^{-1}, the longer the dwelling time, the higher the pull-off force F_p and work of adhesion G due to increased poroelastic diffusion. For these cases, the solvent does not have sufficient time to balance the pressure gradient because the interfacial crack propagates through the whole contact much quicker than solvent diffusion; *e.g.*, $(a/V_c)/\tau_{PE} \sim 1.39 \times 10^{-3}$ for V_u = 10 mm s^{-1} case.

Gelatin samples exhibit only 40% additional enhancement in apparent work of adhesion with increasing dwelling times at high unloading rates. Much larger enhancement was reported on other types of hydrogels.[9,16] For instance, Lai *et al.*[16] reported around 4 fold increase in pull-off forces as a function of holding time for a wide range of indentation depths (4–30 μm) on 10% polyacrylamide (pAAm). Unloading times for their experiments were also much smaller than the poroelastic time constant, which suggests that the above-mentioned suction effect is possible. The contact loads employed in these tests and associated hydrostatic stresses localized to contact can be estimated as $\sigma_{hyd} \approx$ 2–5 kPa, which is smaller than the osmotic pressures reported for polyacrylamide $\Pi_{pAAm} \approx$ 11 kPa.[6] Poroelastic diffusion will be negligibly small under these loading conditions[6,42] and thus cannot explain the observed enhancement. This also corroborates with Lai *et al.*[16]'s proposal for the mechanism of enhancement: hydrophobic backbone of the polyacrylamide and polystyrene probe pushes the water away from the interface only locally and facilitates more solid–solid bonding. We do not anticipate a similar mechanism in our study as both the glass probe and gelatin samples are hydrophilic. In our tests, the maximum hydrostatic stress beneath the contact is approximately $\sigma_{hyd} \approx$ 1.1 kPa for all cases, where $\Pi_{gel} \approx$ 1 kPa.[43] For the fast unloading cases, water does not have time to diffuse back and balance the pressure gradient caused by unloading, and thus the suction effect is expected. This can be quantified by the ratio of crack propagation time and poroelastic relaxation time constant; *i.e.*, $(a/V_c)/\tau_{PE}$, which is 1.17×10^{-2} and 1.39×10^{-3} for V_u = 1 and 10 mm s^{-1}, respectively, and thus very negligible back-diffusion is expected to occur in these cases. Reale *et al.*[9] reported a 5-fold increase in apparent work of adhesion on polyacrylamide gels with increasing dwelling times. In their tests, the maximum hydrostatic stress beneath the contact is around $\sigma_{hyd} \approx$ 18 kPa $> \Pi_{pAAm} \approx$ 11 kPa; *i.e.*, larger areal fraction beneath the probe experiences poroelastic suction upon unloading compared to our tests, explaining the greater dwelling-time-induced enhancement compared to ours. Since gelatin exhibits a more brittle response than polyacrylamide,[44,45] increasing contact pressures to much greater values than osmotic pressure can lead to local failure, and complicate the mechanical response at pull-off.

Another influence of t_{dwell} on gel adhesion could be the change in the solvent/solid fraction around the contact. Increasing t_{dwell} means more solvent diffusion away from the contact, and thus relatively higher solid fraction beneath the probe. When surface energies between the probe-on-solvent and probe-on-solid network differ considerably, such changes in solid fraction can influence the total work of adhesion. For instance, Jha *et al.*[46] showed the influence of areal oil-fraction on work of adhesion measured on glass-on-PDMS (polydimethylsiloxane) swollen with silicone oil at different fractions. This influence is expected to be minute for the gelatin samples that we studied here. This is because the surface energies reported for collagen films extracted from various sources (31.4–38.6 mN m^{-1}, ref. 47) and 4% porcine gelatin gels (37.5 mN m^{-1}, ref. 48) are very close and thus relative areal fraction of the solid/solvent is not expected to change the work balance at different dwelling times.

4 Conclusion

In this work, we investigated rate-dependent adhesion and its relation to the poroviscoelastic response of gelatin. In particular, we conducted adhesion tests on gelatin samples *via* a custom-built spherical glass probe tack tester and an *in situ* imaging module, and revealed correlations between poroviscoelastic relaxations and the enhancement of work of adhesion. We controlled the unloading rates to achieve a broad range of crack (contact edge) velocities that were below the sonic regime, and observed an order of magnitude enhancement in the work of adhesion. Power-law scaling between the enhancement of work of adhesion and crack velocities followed closely the scaling of work of fracture in viscoelastic materials (the Persson and Brener model). The vertical extensions that we found during adhesion tests scaled linearly with the enhancement of work of adhesion. Similar scaling was predicted for the crack tip radius and work of fracture in viscoelastic medium; validating the viscoelastic deformations, and associated dissipation and crack tip kinematics govern the observed rate-dependent enhancement of adhesion in gelatin. We also varied the dwelling times and thus the degree of poroelastic diffusion beneath the probes, and studied their influence on adhesion. We observed about 40% additional enhancement of the work of adhesion with increasing dwelling times for fast cracks. For slow cracks, the dwelling times did not influence the work of adhesion. These observations were in line with the suction effect previously reported elsewhere: when the interfacial cracks are faster than diffusion rates, the solvent does not have sufficient time to balance the pressure gradient and this leads to an increase in adhesion. Pull-off and contact forces that we employed lead to hydrostatic stresses sligthly greater than the osmotic pressure of the gelatin. Therefore, the dwelling-time-induced enhancement is minute compared to the viscoelastic enhancement. In summary, our results point at viscoelastic relaxations as the dominant mechanism governing the rate-dependent enhancement of adhesion in gelatin. Therefore, tuning the relaxation spectrum of gels by chemistry, concentration and ambient conditions could provide a desirable rate-dependence in adhesion. Since adhesion and friction are inherently correlated to each other for soft multiphasic materials, *e.g.* ref. 12, tuning the friction response is also possible in a similar fashion.

Author contributions

W. L.: conceptualization, methodology, data curation, investigation, and writing – original draft and revisions; M. E.:

conceptualization, supervision, methodology, funding acquisition, and writing – revisions. Both authors checked and approved the submitted version.

Conflicts of interest

There are no conflicts to declare.

Acknowledgements

This work is partially funded by the National Science Foundation (Award No. CMMI-2224380).

Notes and references

1 T. Baumberger, C. Caroli and D. Martina, *Nat. Mater.*, 2006, **5**, 552–555.
2 Z. Zhang, T. Chao and S. Jiang, *J. Phys. Chem. B*, 2008, **112**, 5327–5332.
3 J. D. Ferry, *Viscoelastic properties of polymers*, John Wiley & Sons, 1980.
4 R. S. Lakes, *Viscoelastic materials*, Cambridge university press, 2009.
5 A. H.-D. Cheng, *Poroelasticity*, Springer, 2016, vol. 27.
6 K. D. Schulze, S. M. Hart, S. L. Marshall, C. S. O'Bryan, J. M. Urueña, A. A. Pitenis, W. G. Sawyer and T. E. Angelini, *Biotribology*, 2017, **11**, 3–7.
7 E. P. Chan, Y. Hu, P. M. Johnson, Z. Suo and C. M. Stafford, *Soft Matter*, 2012, **8**, 1492–1498.
8 Y. Lai, D. He and Y. Hu, *Extreme Mech. Lett.*, 2019, **31**, 100540.
9 E. R. Reale and A. C. Dunn, *Soft Matter*, 2017, **13**, 428–435.
10 R. Michel, L. Poirier, Q. van Poelvoorde, J. Legagneux, M. Manassero and L. Corté, *Proc. Natl. Acad. Sci. U. S. A.*, 2019, **116**, 738–743.
11 F. J. C. Serrano, PhD thesis, Sorbonne université, 2019.
12 G. Han and M. Eriten, *R. Soc. Open Sci.*, 2018, **5**, 172051.
13 E. O. McGhee, S. M. Hart, J. M. Urueña and W. G. Sawyer, *Langmuir*, 2019, **35**, 15769–15775.
14 J. Li, A. Celiz, J. Yang, Q. Yang, I. Wamala, W. Whyte, B. Seo, N. Vasilyev, J. Vlassak and Z. Suo, *et al.*, *Science*, 2017, **357**, 378–381.
15 G. Han, M. Eriten and C. R. Henak, *J. Mech. Behav. Biomed. Mater.*, 2019, **96**, 186–192.
16 Y. Lai and Y. Hu, *Mech. Mater.*, 2021, **159**, 103877.
17 D. Labonte and W. Federle, *Soft Matter*, 2015, **11**, 8661–8673.
18 L. Liu, K. Yerrapragada, C. R. Henak and M. Eriten, *J. Vib. Acoust.*, 2022, **144**, 051003.
19 A. M. Esfahani, J. Rosenbohm, B. T. Safa, N. V. Lavrik, G. Minnick, Q. Zhou, F. Kong, X. Jin, E. Kim and Y. Liu, *et al.*, *Proc. Natl. Acad. Sci. U. S. A.*, 2021, **118**, e2019347118.
20 R. A. Schapery, *Int. J. Fract.*, 1975, **11**, 141–159.
21 C.-Y. Hui, D.-B. Xu and E. J. Kramer, *J. Appl. Phys.*, 1992, **72**, 3294–3304.
22 J. Greenwood and K. Johnson, *Philos. Mag. A*, 1981, **43**, 697–711.
23 J. Greenwood, *J. Phys. D: Appl. Phys.*, 2004, **37**, 2557.
24 P.-G. de Gennes, *Langmuir*, 1996, **12**, 4497–4500.
25 B. Persson and E. Brener, *Phys. Rev. E: Stat., Nonlinear, Soft Matter Phys.*, 2005, **71**, 036123.
26 B. Persson, *Tribol. Lett.*, 2021, **69**, 115.
27 C. Müller and M. Müser, *J. Chem. Phys.*, 2023, **159**, 234705.
28 A. Khakalo, I. Filpponen and O. J. Rojas, *Biomacromolecules*, 2017, **18**, 1426–1433.
29 T. Baumberger, C. Caroli and D. Martina, *Eur. Phys. J. E: Soft Matter Biol. Phys.*, 2006, **21**, 81–89.
30 F. J. Cedano-Serrano, U. Sidoli, A. Synytska, Y. Tran, D. Hourdet and C. Creton, *Macromolecules*, 2019, **52**, 3852–3862.
31 A. C. Dunn, A. A. Pitenis, J. M. Urueña, K. D. Schulze, T. E. Angelini and W. G. Sawyer, *Proc. Inst. Mech. Eng., Part H*, 2015, **229**, 889–894.
32 L. Afferrante and G. Violano, *J. Mech. Phys. Solids*, 2022, **158**, 104669.
33 K. L. Johnson, K. Kendall and A. Roberts, *Proc. R. Soc. London, Ser. A*, 1971, **324**, 301–313.
34 G. Violano, A. Chateauminois and L. Afferrante, *Front. Mech. Eng.*, 2021, **7**, 664486.
35 I. Naassaoui, O. Ronsin and T. Baumberger, *Extreme Mech. Lett.*, 2018, **22**, 8–12.
36 H. H. Winter and F. Chambon, *J. Rheol.*, 1986, **30**, 367–382.
37 H. Winter, Permanent and Transient Networks, 1987, pp. 104–110.
38 S.-h Hsu and A. M. Jamieson, *Polymer*, 1993, **34**, 2602–2608.
39 V. Kokol, Y. B. Pottathara, M. Mihelčič and L. S. Perše, *Colloids Surf., A*, 2021, **616**, 126356.
40 J. Ahmed, *Advances in food rheology and its applications*, Elsevier, 2017, pp. 377–404.
41 M. H. Müser and B. N. Persson, *Europhys. Lett.*, 2022, **137**, 36004.
42 T. Shoaib and R. M. Espinosa-Marzal, *Tribol. Lett.*, 2018, **66**, 96.
43 J. H. Northrop and M. Kunitz, *J. Gen. Physiol.*, 1926, **10**, 161–177.
44 K. Yerrapragada, D. Chawla, C. R. Henak and M. Eriten, *Exp. Mech.*, 2022, 1–10.
45 J. Li, W. R. Illeperuma, Z. Suo and J. J. Vlassak, *ACS Macro Lett.*, 2014, **3**, 520–523.
46 A. Jha, P. Karnal and J. Frechette, *Soft Matter*, 2022, **18**, 7579–7592.
47 M. Michalska-Sionkowska, O. Warżyńska, B. Kaczmarek-Szczepańska, K. Łukowicz, A. M. Osyczka and M. Walczak, *Materials*, 2021, **14**, 1322.
48 R. Wang and R. W. Hartel, *Food Hydrocolloids*, 2022, **124**, 107132.

